URANS AND LES COMPUTATIONS FOR THE HEAT TRANSFER CHARACTERISTICS OF WALL BOUNDED BUOYANT FLOWS

Constantinos Katsamis[1*], Tim J. Craft[1], Hector Iacovides[1], Juan Uribe[2]
[1]Department of Mechanical, Aerospace and Civil Engineering, University of Manchester, M13 9PL,UK
[2]EDF Energy R&D UK Centre, Manchester, United Kingdom

ABSTRACT

The present investigation provides an insight on the heat transfer characteristics of a differentially heated square cavity at a high Rayleigh number ($= 10^{11}$) through the use of advanced URANS models and a wall-resolved Large Eddy Simulation (LES). The performance of the cost-effective RANS, using high-Reynolds-number (HRN) as well as low-Reynolds-numbers (LRN), turbulence closures is assessed. The models include both eddy-viscosity schemes and a second-moment closure which either fully resolve the viscous sublayer or adopt a recently developed numerical variant of the Analytical Wall Function (AWF) to approximate the wall shear stress and heat flux. Further, a computationally demanding wall-resolved LES is compared against the time-dependent 3D RANS simulations which enhances understanding on the transition phenomenon in the flow and provides an indication on the grid resolution requirements at such a high Rayleigh number.

1. INTRODUCTION

The forthcoming generation of nuclear reactors is anticipated to consist of smaller, safer, and more reliable units which are expected to depend strongly on natural circulation. This has drawn the attention of many thermohydraulic researchers in extensively studying a range of cooling configurations, amongst them being the buoyancy-driven flow inside a deep square cavity, in which the unsteadiness and the transitional turbulent boundary layer regions challenge most RANS and LES strategies. A few numerical investigations can be found which present deviations between the predictions of each strategy in modelling the flow in a square cavity at Rayleigh number (Ra) of 1.58×10^9 [1, 2, 3]. The study by [4] examined RANS-based methods and revealed the predictive deficiency of the low-Re $k-\varepsilon$ Launder and Sharma (LS) model of [5], which returned a fully laminar flow. On the other hand, the high-Re models tested, both eddy viscosity and second moment closures, combined with the Analytical Wall Function (AWF) of [6] returned more accurate flow representations. This advanced wall treatment was highly recommended for modelling this flow in which the near-wall velocity profile no longer obeys the logarithmic law. The study also compared the effective diffusivity approach for the turbulent heat flux vector ($\overline{u'_j t'}$) against more elaborate approaches, including the Generalised Gradient Diffusion Hypothesis and an Algebraic Heat Flux model which includes direct effects of buoyancy and the anisotropy of the turbulence field. Recently, DNS data of flow in a square cavity at a range of Rayleigh numbers (Ra= $10^8 - 10^{11}$) for air (Prandtl $= \mu c_p / \lambda = 0.71$), have been made available by Sebilleau et al. (2018) [7]. The DNS study provides detailed statistics of the first and second order moment quantities. It was observed that raising Ra causes the velocity boundary layers along the vertical walls to become thinner and the laminar proportion of the core region to become larger.

The present contribution aims to provide an assessment on the cost effectiveness and the capabilities of commonly adopted RANS models, and a wall-resolved LES approach, in the prediction of the flow and thermal development in the differentially heated square cavity of [7]. Different wall treatments, including a new more general version of the AWF, and different heat flux models, are also examined within the RANS models.

2. MATHEMATICAL FRAMEWORK AND TURBULENCE MODELLING

The heated flow within the cavity induces density variations that generate local imbalances between the pressure gradient and the gravitational body forces, leading to the buoyancy-driven motion. Assuming that the density varies little about its reference value ρ_{ref}, so $|\rho - \rho_{ref}| / \rho_{ref} \ll 1$, the Boussinesq approximation can be invoked for the local body force which depends now on the volumetric thermal expansion coefficient β, the imposed temperature difference ($\Delta T = T_h - T_c = 5K$) and the gravity vector, g_j:

*Corresponding author: constantinos.katsamis@manchester.ac.uk (Constantinos Katsamis)

$$F_j^b = -\rho_{ref} g_j(\beta(T - T_{ref})) \quad (1)$$

To match the DNS of [7] the flow field has been simulated at Ra $= \rho g \beta \Delta T H^3 / \mu\alpha = 10^{11}$. The open-source code, *Code_Saturne v5.0.8*, developed by EDF Energy, is chosen to solve the unsteady transport equations of mass, momentum and energy using the Finite Volume Method [8]. Spatial discretisation is handled using second-order upwind based discretization schemes for the temperature and velocity, with dynamic switching to 1st order where necessary, and upwind for the turbulent quantities in the RANS simulations. The second order central difference scheme is used alongside the LES with SIMPLEC for the pressure algorithm.

In the LES strategy, the code adopts the grid size Δ to spatially filter the transport equations. In the present study, the Dynamic Smagorinsky-Lilly model has been employed, which follows the proposal of [9,10] that applies a second test filter, in order to define the sub-grid viscosity, ν_{SGS}, to represent the mixing effects of the sub-grid dissipative scales. Thus, the sub-grid scale model uses information from the resolved field, combined with the effective diffusivity, for the sub-grid-scale contribution to the heat fluxes. For comparisons with the RANS model results, time-averaged quantities can then be extracted from the LES, combining the resolved contribution, covering the inertial subrange of the energy spectrum, and the modelled sub-grid-scale contribution:

$$\overline{\phi'\psi'} = \underbrace{\left(\overline{\hat{\phi}\cdot\hat{\psi}} - \bar{\hat{\phi}}\cdot\bar{\hat{\psi}}\right)}_{resolved} - \underbrace{\overline{\phi'\psi'}}_{SGS\ modelled} \quad (2)$$

where caret symbol ^ denotes the filtering operation and overbar ¯ the time-averaging.

RANS models require significantly less computational resources than LES, albeit it at some expense of accuracy, depending on the model employed. Eddy viscosity models (EVMs), such as the HRN $k-\varepsilon$ of [11] or the LRN $k-\varepsilon$ *LS* model [5] tested here, utilise an eddy viscosity ν_t ($\propto c_\mu k^2/\ \varepsilon$) in order to linearly relate the Reynolds stresses ($\overline{u_i' u_j'}$) that arise from Reynolds-averaging with the mean strain rates. A more elaborate closure strategy is followed by the LRN EBRSM of [12, 13], also tested in the present work, which solves a transport equation for each of the 6 components of $\overline{u_i' u_j'}$ and one for the dissipation rate. The EBRSM is formulated based on the elliptic relaxation concept to blend outer region and the near-wall forms of the pressure strain redistribution term by solving an additional differential equation for the blending parameter α, which is used to define the wall normal vector. The heat flux models adopted for the RANS models are the effective diffusivity approach for the EVMs, the Generalised Gradient Diffusion Hypothesis (GGDH) and a more elaborate form, that of the algebraic flux model (AFM) for the RSM (see [14]). The AFM also requires the solution of a transport equation for the temperature variance. The RANS models are all applied in unsteady simulations, as the flow is expected to contain large-scale unsteadiness, and for comparisons with the LES (and DNS) the computed moments of the fluctuations then need to account for both the resolved unsteady motions and the modelled turbulence:

$$\overline{\phi'\psi'} = \underbrace{\overline{\phi''\psi''}}_{modelled} + \underbrace{(\overline{\langle\Phi\rangle\cdot\langle\Psi\rangle} - \overline{\langle\Phi\rangle}\cdot\overline{\langle\Psi\rangle})}_{resolved} \quad (3)$$

1.1 Near-wall modelling

It is well known that the difficulty of simulating buoyant driven flows is mainly due to the near-wall regions where the effects of turbulence mixing and heat transfer are of utmost importance. At such high Ra flow in the square cavity, the viscous sublayer region requires a substantial number of nodes across the near-wall layer to resolve accurately the steep velocity and temperature gradients there. The full integration of the governing transport equations down to the solid wall is achieved using the low-Re RANS schemes tested here and the LES, in both cases with near-wall grid y^+ value less than 1.

A more robust strategy is adopted using a wall function, in which approximations for the required wall quantities for the boundary conditions of velocity, temperature and turbulence values for the near-wall cells are provided. From earlier square cavity computations conducted, though not included here, the log-law based wall function has been proved insufficient to model the near-wall physics. This motivated the need to introduce and further develop a numerical form of the Analytical Wall Function (AWF) of [6] in the code utilised. The proposed approach solves numerically a simplified momentum

equation in the wall-normal direction across the near-wall control volume which accounts for buoyancy and convective effects, following the form of:

$$\frac{\partial}{\partial y}\left[(\mu+\mu_t)\frac{\partial U}{\partial y}\right]=\frac{\partial U}{\partial x}-\frac{\partial P}{\partial x}+\rho g_x \tag{4}$$

A linear variation of μ_t is assumed as in [6] and the simplified temperature equation follows a similar form. Since the equation (4) is solved numerically in the AWF, a local value at each sub-grid location based on the sub-grid temperature is used for the buoyancy contribution. Equivalently, the main grid discretized momentum equation in the near-wall cell requires the contribution due to buoyancy to be modified, replacing the point-wise value with a more accurate approximation of the cell-averaged one as:

$$\overline{F_j^b}=\frac{1}{y_n}\int_0^{y_n}\rho_{ref}g_j\beta(T-T_{ref})dy\approx\frac{1}{y_n}\rho_{ref}g_x\beta\sum_{j=1}^{n-1}(T_j-T_{ref})\Delta y \tag{5}$$

where T_j denotes the temperature from the 1D subgrid solution. A similar route is followed for the cell-averaged contributions of the production of k due to shear (P_k) and due to buoyancy (G_k) in the main grid.

1.2 Grid resolution and computational cost

The grid resolution and the computational resources required along with the time utilised to conduct the wall-resolved LES are compared against those of the 3D URANS and provided in Figure 1 and Table 1. The cavity dimensions used are the same with those of the DNS and information on the time-step adopted for each case are included. It is worth mentioning that an initial time step was estimated in RANS to resolve circulations around the cavity, based on the cavity length scale and buoyant velocity scale, which was then refined to satisfy a CFL≤ 1. For the time discretization scheme, the 1st order semi-implicit was used in RANS whereas the LES adopts the second-order Crank-Nicholson scheme.

It must be highlighted that based on the criterion proposed by [15] the LES resolves sufficiently the large inertial subrange and a portion of the smallest dissipative scales in the flow (LESIQ=0.95). Clearly, the LES with 14.6 million nodes is far less expensive compared to the 726 million nodes utilised in the DNS. However, it is clear that the URANS computations are by far the cheapest and least demanding option in terms of number of CPUs, time and knowledge required to conduct the simulations. As shown, modelling the viscous sublayer effects using a LRN model takes nearly eleven times longer than employing the AWF with a coarser near-wall grid, in the 3D computations. Solving for each Reynolds-Stress component and the temperature variance in the EBRSM AFM scheme has shown around 30% rise in the computational cost compared to the LRN two-equations alternative.

Table 1: Computational resources consumed in the present LES and URANS simulations

Case	LES (*Dynamic Smagorinsky*)	low-Re $k-\varepsilon$ *LS*	high-Re $k-\varepsilon$ *AWF*
$L\times H\times D$	$1\times1\times0.15$	$1\times1\times0.15$	$1\times1\times0.15$
$N_L\times N_H\times N_D$	$352\times594\times70$	$250\times250\times20$	$100\times100\times20$
$\Delta x^+\times\Delta y^+\times\Delta z^+$	$(<51)\times<1\times<22$	$y^+<1$	$y^+>25$
$\Delta t[s]$	0.00106	0.0106	0.0106
CPUs	512	16	16
Computational time [hrs]	1464	391.5	35.5

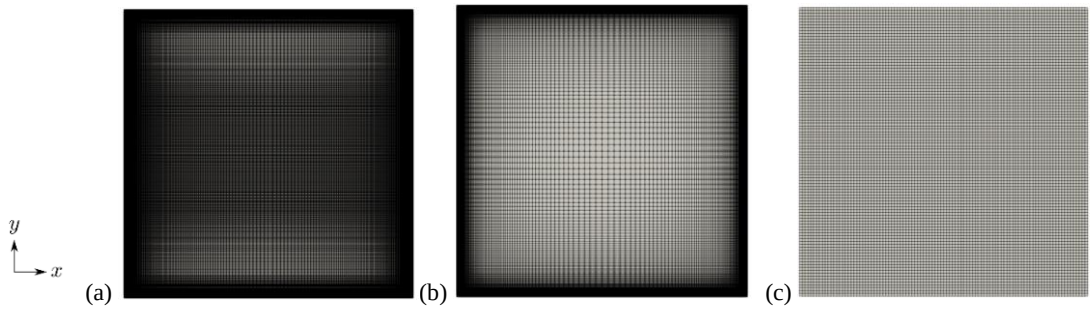

Figure 1: Meshes for the (a) LES, the (b) LRN and (c) HRN RANS models of the 3D square cavity at $Ra=10^{11}$.

3. DATA ANALYSIS

The thermal field in the differentially heated square cavity exhibits buoyant plumes being injected into the motionless stratified core from the corner regions according to the non-dimensional instantaneous temperature contour plot of the LES shown in Figure 2 (a). It is evident that the thermal fluctuations due to turbulence are confined to the near-wall regions according to the LES. The *EBRSM* and the $k-\varepsilon\ AWF$ model only resolved large scale flow instabilities, which can be seen to be occur in the two opposite corners, at the bottom left and top right of the cavity (see Figure 2 (b)-(c)). Along the two active walls, the fluids ascends as it is heated, or descends as it is cooled, and the subsequent acceleration leads to high velocity gradients in the near-wall regions. Subsequently, this leads to transitional turbulent boundary layer regions being developed along both active walls. A detailed representation of the structures in those unsteady boundary layers is revealed from the non-dimensional instantaneous velocity magnitude contour plot of the LES in Figure 3 (a). As shown in Figure 3, the $k-\varepsilon\ AWF$ returns a more representative thickness of those near-wall layers along the active walls in comparison with the more complex *EBRSM AFM* which returns thinner regions.

The transition phenomenon is a real challenge for URANS models and LES, and its prediction is sensitive to both the grid density and the time step size. In the LES, the non-uniform grid was carefully refined around that region to capture the phenomenon sufficiently and enable the large-scale structures to fully develop. Figure 4 (a) demonstrates the capability of the LES in capturing the transition phenomenon at $y/H \approx 0.2$-0.4 according to the large-scale structures presented in the form of Q-criterion $(1/2(\Omega_{ij}\Omega_{ij}-S_{ij}S_{ij}))$ coloured by the non-dimensional velocity magnitude. Turning attention to the quantitative data of the second moments, the turbulence levels are shown to grow stronger after the transition has occurred, at $y/H=0.5$ in Figure 4 (b), consistent with what the structures in Figure 4 (a) suggest. At locations $y\ /\ H$ of 0.1 and 0.5, the near-wall k levels returned by the $k-\varepsilon\ AWF$ 3D and EBRSM GGDH are closer to the LES and DNS values than those of the low-Re $k-\varepsilon\ LS$ 3D and the $EBRSM\ AFM$ 3D (see Figure 4 (b)). The latter LRN schemes tend to slightly underestimate the buoyancy and shear turbulence generation, leading to them returning a slightly too thin near-wall turbulent region. The LES computation clearly outperforms all four RANS schemes, returning k levels that collapse with the DNS profiles.

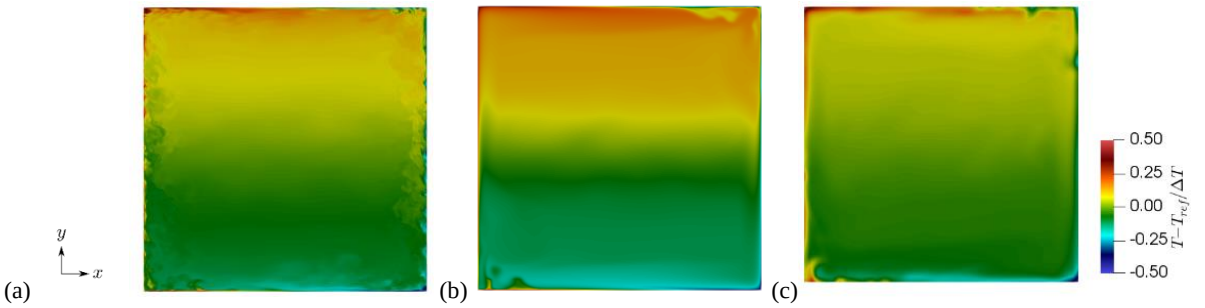

Figure 2: Mid-plane of the non-dimensional temperature contour from the (a) *Dynamic Smagorinsky LES*, the (b) *EBRSM AFM* and the (c) $k-\varepsilon\ AWF$ in the square cavity at $Ra=10^{11}$.

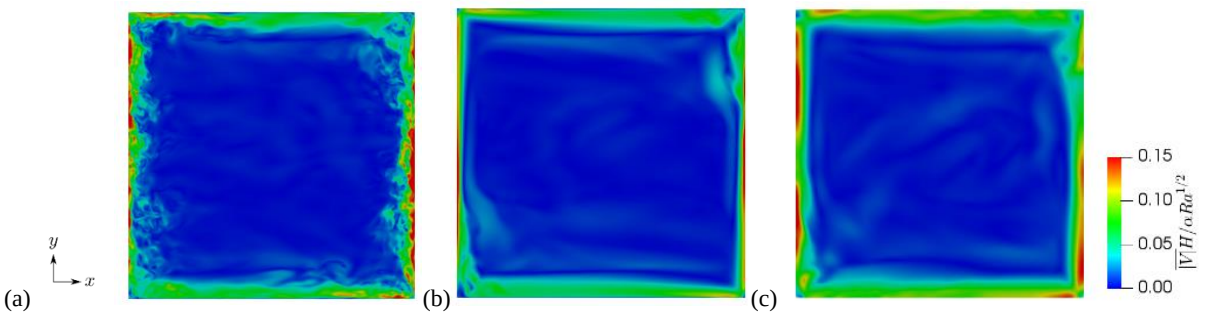

Figure 3: Mid-plane of the non-dimensional velocity magnitude contour from the (a) *Dynamic Smagorinsky LES*, the (b) *EBRSM AFM* and the (c) $k-\varepsilon\ AWF$ in the square cavity at $Ra=10^{11}$.

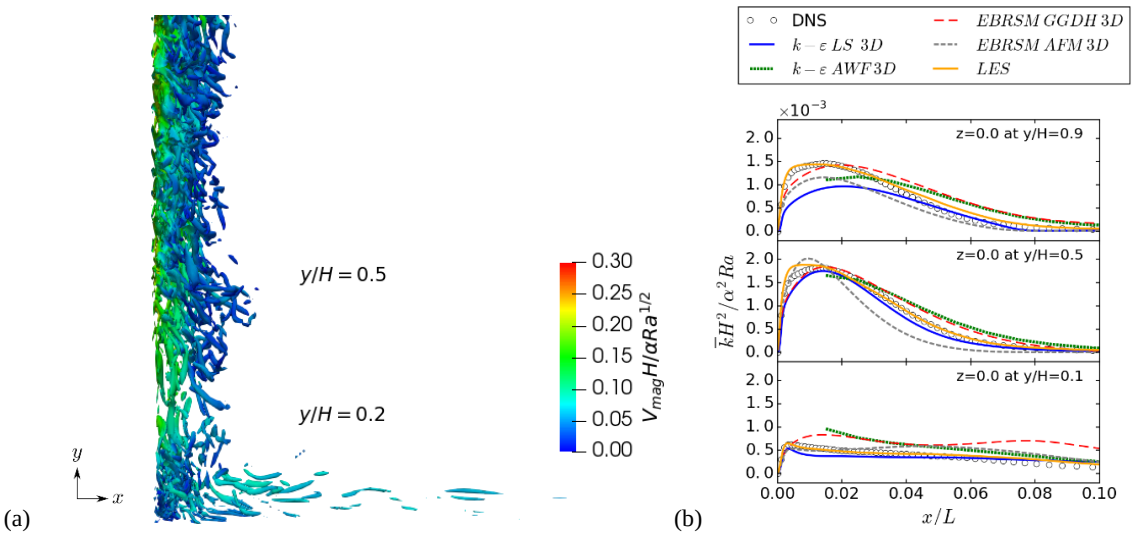

Figure 4: (a) Q-criterion at the hot wall boundary layer from the LES of the square cavity, coloured with the non-dimensional velocity magnitude. (b) Non-dimensional k profiles for the 3D URANS models and the LES.

Figure 5 (a) presents comparisons between the predictions of the time-averaged Nusselt number ($= q_w L/\lambda\Delta T$) profile along the hot wall of the cavity and the DNS. As expected, the LES outperforms the URANS and returns a profile very close to that of the DNS, following closely the turbulence enhancement of the Nu distribution of the DNS. It is evident from the profile and the thermal structures observed earlier in the thermal field of Figure 2 (a) that on the hot wall the laminar to turbulent transition point occurs at around $y\ /\ H \approx 0.2 - 0.4$. The LRN $k-\varepsilon$ *LS* follows the DNS Nu profile closely beyond $y\ /\ H \approx 0.4$, although for $y\ /\ H < 0.4$ it underestimates the levels in the laminar and transitional regions. In contrast, the *EBRSM* with the AFM for the $\overline{u'_J t'}$ returns a distribution with a similar shape to the DNS but slightly overestimated beyond the turbulent transition point. The EBRSM with GGDH approach returns a Nu profile that is shifted much higher than that of the DNS. The high-Re $k-\varepsilon$ with the proposed approach of the numerical AWF results in an Nu distribution that is not far off the data (less than 15%), though at y/H=0.4, after the turbulence transition occurs, the AWF does not capture the local maximum of the DNS. The returned non-dimensional $\overline{u'_J t'}$ from the LES in Figure 5 (b) shows a small deviation from the DNS at all three locations shown, though its performance is far better than the RANS predictions. Nevertheless, the $k-\varepsilon$ in conjunction with the effective diffusivity formulation for $\overline{u'_J t'}$, especially the $k-\varepsilon$ *LS* scheme, results in values that are generally reasonably close to the DNS. The returned $\overline{u'_J t'}$ profile from the *EBRSM* with either heat flux approximation, *GGDH* or *AFM*, largely agrees with the data at the $y/\ H$=*0.9* location, whilst at the lower locations the models show larger deviations.

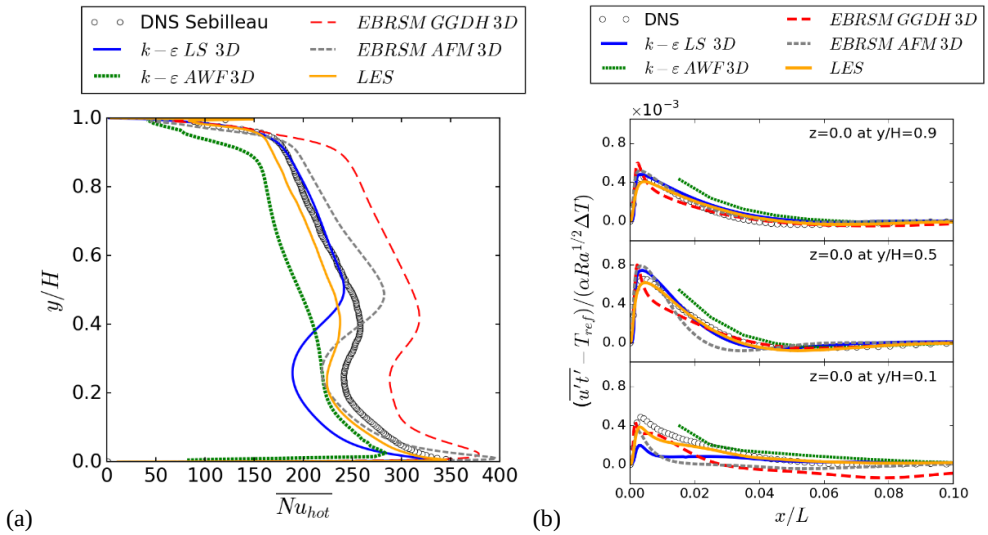

Figure 5: (a) Hot wall local Nusselt number and (b) non-dimensional $\overline{u't'}$ profiles for the 3D URANS models and the LES.

4. CONCLUSIONS

In the present investigation, three URANS models and a wall resolved LES are assessed in terms of modelling the near-wall mixing and heat transfer effects of a differentially heated square cavity. At $Ra = 10^{11}$ the core remains largely stagnant and laminar whereas large scale unsteadiness is observed along the thin boundary layers of the vertical walls. The LES predicts sufficiently accurately the flow and thermal field, returning the correct behaviour of the overall Nu, k and $\overline{u't'}$ distributions compared to the DNS. As far as the three low-Re models are concerned, they return Nu values close to that of the data, except for the *EBRSM GGDH* which overestimates the Nu levels. The HRN $k-\varepsilon$ *AWF* with a much coarser near-wall grid tends to be not far off the data. The predicted k and $\overline{u't'}$ from the RANS models are not so far off the data, even when the effective diffusivity approach is used. The predictions of the near-wall turbulence and heat transfer effects from the AWF approach are shown to be highly competitive to those of the LRN alternatives. Overall, the LES is proved the most accurate strategy for modelling natural convection flows that involve transitional phenomena, however the computational resources, the time and knowledge required to conduct such a simulation make the RANS approaches more preferable for industrial application. The work presents a major contribution in the simulation of a natural convection flow within square cavities at a high Ra which is relevant to passive cooling applications of large systems. The results make a strong addition to the relatively old database that mostly concerns the low-Ra regime in such cavities and are sufficiently fundamental to be useful in a range of application fields involving natural or forced convection flows. The conclusions drawn thus far encourage further computations of the AWF with a Reynolds stress transport model, and LES with different sub-grid scale models to examine their predictive effectiveness.

ACKNOWLEDGEMENTS

The author would like to acknowledge the funding of MACE Beacon Scholarship of The University of Manchester and EDF Energy. The assistance given by Research IT, and the use of The HPC Pool funded by the Research Lifecycle Programme at The University of Manchester are also acknowledged.

REFERENCES

[1] Kumar R., and Dewan A., A study of LES-SGS closure models applied to a square buoyant cavity. *In. J. of Heat & Mass Transfer*, **98** (2016)164-175.

[2] Clifford C. E., Kimber M. L., Assessment of RANS and LES turbulence models for natural convection in a differentially heated square cavity, *Numerical Heat Transfer*; Part A: Applications **78** (10) (2020) 560.

[3] Salinas-Vázquez, W. Vicente, E. Martínez, E. Barrios, Large eddy simulation of a confined square cavity with natural convection based on compressible flow equations, *In. J. of Heat and Fluid Flow* **32** , 5, (2011) 876-888.

[4] Omranian A., Craft T. J., Iacovides H., The computation of buoyant flows in differentially heated inclined cavities, *In. J. of Heat & Mass Transfer* **77** (2014) 1-16.

[5] Launder, B. E. and Sharma, B. I., Application of the energy-dissipation model of turbulence to the calculation of flow near a spinning disc. *Letters in Heat and Mass Transfer*, **1** (2) (1974) 131-137.

[6] Craft T. J., Gerasimov A. V., Iacovides H., & Launder B. E., Progress in the generalization of wall-function treatments. *In. J. of Heat & Fluid Flow*, **23** (2002) 148–160.

[7] Sebilleau F., Issa R., Sylvain L. & Walker S. P., Direct Numerical Simulation of an air-filled differentially heated square cavity with Rayleigh numbers up to 10^{11}, *In. J. Heat & Mass Transfer* **123** (2018) 297-319.

[8] Archambeau F., Méchitoua N., and Sakiz M., Code Saturne: A Finite Volume Code for the computation of turbulent incompressible flows– Industrial Applications. *In. J. on Finite Volumes* **1** (2004) 1-62.

[9] Smagorinsky, J., General Circulation Experiments with the Primitive Equations. *Monthly Weather Review*, **91** (1963): 99-164.

[10] Lilly D. K., A proposed modification of the Germano subgrid-scale closure method. *Physics of Fluids* A**4** (1992) 633.

[11] Launder, B. E. and Spalding, D., The numerical computation of turbulent flows. *Computer Methods in Applied Mechanics and Engineering*, **3** (2) (1974) 269-289.

[12] Manceau R., Hanjalić, K., Elliptic blending model: A new near-wall Reynolds-stress turbulence closure, *Physics of Fluids* **14** (2002) 744-754.

[13] Manceau R., Recent progress in the development of the Elliptic Blending Reynolds-Stress model, *In. of Heat and Fluid Flow*, **51** (2015) 195-220.

[14] Hanjalic, K., Kenjeres, S. and Durst, F., Natural convection in partitioned two-dimensional enclosures at higher Rayleigh numbers. *In. J. of Heat and Mass Transfer* **39** (1996) 1407-1427.

[15] Klein, M. Meyers, J. and Geurts, B. J., Assessment of LES quality measure using the error landscape approach. *ERCOFTAC Series*, **12** (2008) 131-142.